International Journal of Advanced Engineering Research and Science (IJAERS)
Peer-Reviewed Journal
ISSN: 2349-6495(P) | 2456-1908(O)
Vol-10, Issue-9; Sep, 2023
Journal Home Page Available: https://ijaers.com/
Article DOI:https://dx.doi.org/10.22161/ijaers.109.1

Analysis of distortion, corrosion and mechanical properties of welded ASTM A36 steel U-type profiles

Josemairon Prado Pereira[1*], Bruno Agostinho Hernandez[2], Gilberto de Magalhães Bento Gonçalves[3], Edson Antonio Capello Sousa[4] and Jonatas Martins Pereira[5]

[1,2,3,4]School of Engineering, Department of Mechanical Engineering, São Paulo State University "Júlio de Mesquita Filho" (UNESP) – [5]School of Engineering, Department of Civil Engineering, São Paulo State University "Júlio de Mesquita Filho" (UNESP) – Campus Bauru, Av. Luiz Edmundo Carrijo Coube, b. 14-01 - Vargem Limpa - 17033-360 - Bauru, SP - Brazil

Received: 21 Jul 2023,

Receive in revised form: 29 Aug 2023,

Accepted: 06 Sep 2023,

Available online: 14 Sep 2023

***Keywords*— Distortion. Mechanical properties. Corrosion. Welded joint. Metallic structures.**

***Abstract*—** *Several factors affect the performance, manufacturing, and assembly of metallic profiles: equipment, welding parameters, and consumables. ASTM A36 steel profiles are widely used to obtain high-quality welded joints. Three factors in the welded joints need to remain nearly invariable and within predictable limits: distortion, corrosion, and mechanical properties. However, industries still have problems with welding steel profiles, such as warping misalignment, misfit, and poor mechanical properties. As a result, it is necessary a calibrated and affordable methodology for welding ASTM A36 steel profiles on the factory floor. Therefore, this study aims to analyse the mechanical performance of ASTM A36 steel profile welded joints using a robot welding machine. A GMAW (Metal Active Gas) welding process was applied to an ASTM A36 type U 100 x 50 profile, 3.0 mm thick, employing a Motoman UP6 robotic arm in butt joints, with and without dots. Two different rod electrode types were used (AWS ER70S-3 and ER70S-6), with a 75%Ar/25%CO2 shielding gas and current density welding set at 160.6 A and 20.5 V. A three-dimensional scanning methodology was adopted to investigate welded joint distortions. While salt spray accelerated corrosion test was used to analyse deterioration. The mechanical properties were analysed by macrography, microhardness, and chemical analyses in the Heat Affected Zone (HAZ). It was found a distortion displacement lower than 450 µm on the sample's surface, and a mass loss of 10.1 µm/year was detected in terms of corrosion resistance. There was also evidence of chemical heterogeneity between the base metal and weld, mainly in the manganese content with an average reduction of 13% in microhardness measurements when AWS ER70S-3 electrode was used. By using calibrated welding parameters and a welding robot, it was possible to obtain mechanically resistant high-quality standardised welds. This procedure can be further improved by using other profile types to implement new robotic welding procedures.*

I. INTRODUCTION

Welding is widely used in structural steel profiles [1]. In order to achieve high-quality welded joints, three factors must remain stable: welded joint distortion, corrosion, and joint mechanical properties.

Distortion in welding is the result of internal stresses and deformations that act on the weld metal and its

surroundings imposed by the welding thermal cycle [2]. Excessive distortions during welding may cause warping and misalignment in part assembly, leading to misfitting and wrong positioning of the profiles, thus compromising the structure's reliability [3-4]. The correct definition of welding procedures, parameters, and sequence is critical for controlling welding-induced distortion, which was previously investigated [5].

Corrosion is another relevant factor that requires continuous attention to ensure that corrosion levels and mass loss stay below 400 µm/year [6]. In critical situations, where metallic structures are constantly attacked by saline or acidic environments (for example, at sea level or in chlorine vapours environments in industries), efforts to stop material mass decay are critical [7].

Tensile strength is the paramount parameter in the designing of bars and welded joints withstanding critical loading, as in roofs and buildings [8]. Consequently, there is a necessity for chemical and mechanical properties control of the welded section to ensure the loading capacity and safety of such profiles [9].

Another matter of concern in welded joints of metal profiles is the heterogeneity between the Heat Affected Zone (HAZ) and the fusion zone, caused by the dilution of the chemical composition between these two regions [10]. The interaction of welding consumables and the base material of the profile influences the joints' hardness, which can make the welding joint particularly fragile [11], [12].

Although all these welding parameters are widely known and studies have been conducted at exhaustion, industries still cannot control their occurrence during in situ welding of structural profiles, mainly for ASTM A36 steel profiles – widely used in the construction field. Consequently, a calibrated methodology for measuring and controlling welding in ASTM A36 steel profiles is urgent and necessary. Moreover, the methodology must be applied on the factory floor using equipment already available in it.

Therefore, the aim of this study is to propose a new welding methodology for the ASTM A36 steel U profiles using a robotic arm assisted with real-time data acquisition to measure deformation levels and control heat intake to reduce distortion, misalignment, and warping when welding those profiles in situ using Gas-Shielded Arc Welding (GMAW) with distinct electrode wire types and joint preparation methods..

II. MATERIALS AND METHODS

2.1 Welding Preparation

Two ASTM A36 cold-bent steel U profiles 100x50x85mm, 3.0mm thick, were used as base metals, Fig. 1. Conventional Gas Metal Arc Welding (GMAW) process using the MIGArc 6200i welding machine (Castolin Eutectic, Switzerland) was conducted with a gas mixture of 75%Ar/25%CO2, at a flow rate of 2.1x10-4 m3 /s (12.5 l/min). Table 1 shows the main chemical elements of the base metal and the electrode wires used.

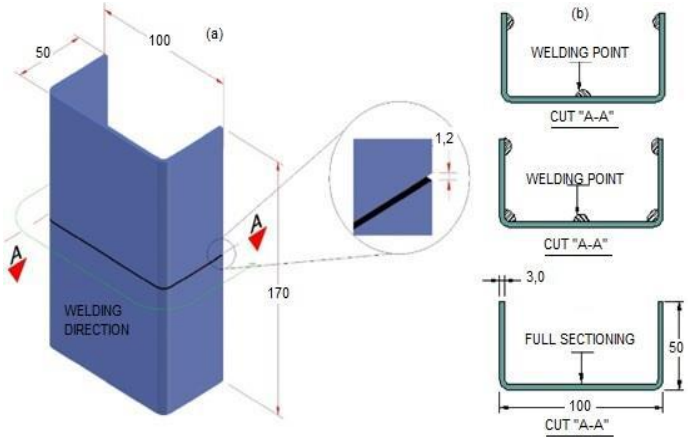

Source: From the authors.

Fig. 1 - Welding joints Assembly: (a) constituent parts arrangement; (b) "U" profiles fixing (cut "AA"). Dimensions in millimetres.

Table 1 - Main chemical elements of base and addition metals.

Material	Composition (% by weight)				
	C	Si	Mn	P	S
ASTM A36	0,11	0,15	0,39	0,013	0,080
ER70S-6	0,10	0,98	1,48	0,012	0,011
ER70S-3	0,09	0,64	1,03	0,012	0,013

Source: From the authors.

Three pre-welding joint techniques were assessed in this study: no pre-welding preparation, three pre-welding joints, and five pre-welding joints. In the latter two cases, the two U profiles were initially pre-welded using the spot-welds technique in odd numbers (three or five) placed along the joint cross-section, Fig. 1. It was assured that the U-profile surfaces were flat, free of inclusions, sanded with sandpaper (80 and 120), and free of oxides or dirt caused by handling.

The influence in welding distortion of two types of electrode rods was also assessed: AWS ER70S-3 and

ER70S-6 electrode wires (with 0.9 mm and 1.0 mm diameters, respectively). Consequently, a total of six (n = 6) combinations of parameters were analysed: U profiles without preparation welded with AWS ER70S-3 or ER70S-6 (SS), U profiles with three spot-welds preparation welded with AWS ER70S-3 and ER70S-6 (3P), and U profiles with five spot-welds preparation welded with AWS ER70S-3 and ER70S-6 (5P). The welding torch was operated by a Motoman UP6 robotic arm (Yaskawa America, Inc., Japan), specially adapted and programmed to carry out the welding operations in a single horizontal movement, always from left to right, Fig. 2.

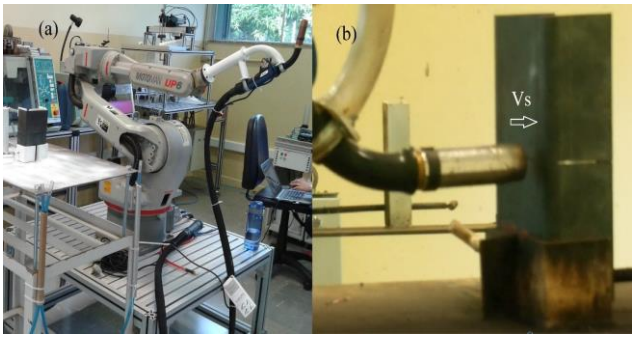

Fig. 2 - Torch displacement system: (a) robotic arm adaptation; (b) joint positioning and welding direction.

Source: From the authors.

During the welding, the instantaneous values of the welding current and voltage were compiled by data acquisition and processing systems. Additionally, the electrode wires' current density was kept around 205 A/mm2 in the welding process. Table 2 lists the average current, voltage, and welding speed for all base metal/electrode wire combinations. The welding bead chemical composition was analysed by optical emission spectrometry Spark OES (PG Instruments Limited, United Kingdom).

Table 2 - Values of the welding parameters applied to the BM/wire-electrode groups

Weld metal	Composition (% by weight)				
	C	Si	Mn	P	S
A36-S6	0,09	0,60	0,86	0,02	0,03
A36-S3	0,09	0,32	0,75	0,02	0,02

Us (voltage), Is (current), Vs (welding speed).

Source: From the authors.

2.2 Distortion Analysis

The distortion analysis due to the welding thermal cycle was carried out using the image superimpose technique of the joint, before and after welding: surface points were collected throughout the joint from images produced by a three-dimensional "OCR" scanner (GOM – Precise Industrial 3D Metrology, Germany). From the collected image data, it is possible to superimpose the images of the joints using Atos Professional surface analysis software (Version V.75S41, GOM – Precise Industrial 3D Metrology, Germany).

2.3 Corrosion Analysis

The corrosion decay rate can be expressed as a function of effective nominal stress (σf) as:

$$\sigma_f = \frac{Q}{A_f} \quad , \text{for } \sigma_f < \sigma_u \qquad (1)$$

Where σu is the ultimate stress, Q is the load applied to the profile and Af is the final area of the profile.

The evaluation of the welded joints' corrosion resistance was carried out in terms of mass loss, according to ASTM B117 standard [21], using an accelerated corrosion test: 189-hours salt spray, with a 5% NaCl solution, at 32 ± 2ºC.

2.4 Macro-structural integrity analysis

The macro-structural integrity was assessed by measuring the width of the obtained weld beads, as well as by

calculating the dilution proportion between Heat Affected Zone (HAZ) and base metal (BM). A 500x industrial desktop magnifyiFig.ng electronic USB digital microscope (v.500x, Imports, China), with Hotviewer software (v.2.0.11.20, HOT Inc., USA), was used to acquire macrograph photos of the welded joint cross sections.

Vickers microhardness tests (loading of 1 kgf) were carried out in a Digimess HV-1000 microhardness testing machine (Digimess, Brazil) to obtain the hardness in the cross-section of the welded joints, covering the weld metal, heat-affected zone, and the base metal. Fig. 3 shows the hardness measurement points spaced 0.25 mm apart to visualize a microhardness field in the weld bead, placed horizontally along three parallel lines in the centre of the weld joint.

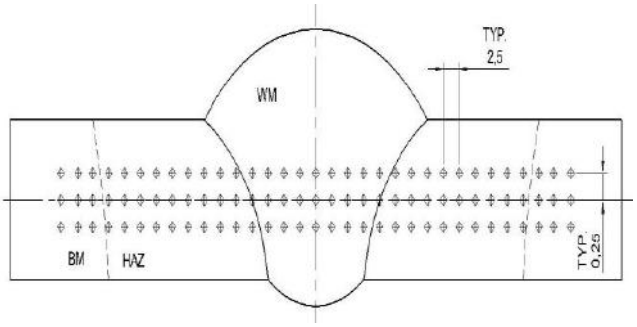

Fig. 3 - Arrangement of the sample's microhardness measurement points. Where HAZ is the Heat Affected Zone, BM is the Base Metal, and WM is the Welding Metal or Fusion Zone.

Source: From the authors.

Ninety-six (n = 96) samples were extracted and machined into standard tensile testing samples (Standard BS 709:1983) [22] from the weld bead region of A-36 steel welded profiles with both ER70-S6 and ER70-S3 electrodes. A tensile test was conducted in an EMIC Universal Testing Machine (Model: 50kN, Instron Equipamentos Científicos Ltda, Brazil) to obtain the mechanical properties of the welding regions.

III. RESULTS

Table 3 lists the chemical element contents of the welded joints obtained during the welding process, and Fig. 4 shows the distortion magnitude mapped by the scanning technique. Welded sets A36-S6 (3P) and A36-S3 (3P) were the least deformed, average of 110 µm. Samples A36-S6 (5P) and A36-S3 (5P) presented an average distortion of 280 µm, whereas samples A36-S6 (SP) and A36-S3 (5P) had the highest deformations, an average of 317 µm.

Table 3 - Contents of basic chemical elements obtained by spectrometry of the weld bead with consumables with electrode wire.

Weld metal	**Composition (% by weight)**				
	C	Si	Mn	P	S
A36-S6	0,09	0,60	0,86	0,02	0,03
A36-S3	0,09	0,32	0,75	0,02	0,02

Source: CADEP.

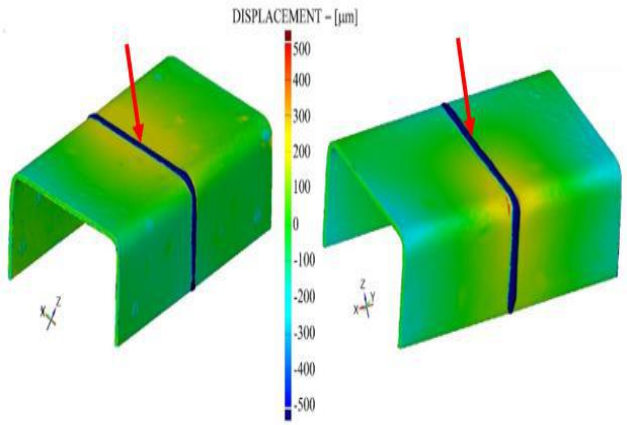

Fig. 4 - Point displacement/distortion: ASTM-S6 and ASTM-S3 welded group. Red Arrow indicates de welding bead.

Source: From the authors.

Fig. 5 depicts the longitudinal displacement/distortion in the cross-section indicated by the red arrow in Fig. 4. The maximum displacement value of 395 µm was observed in the welding process using the electrode wire AWS-ER70-S6, where the welding joint was prepared without spot-welding. The lowest value, 119 µm, was with the same electrode but in the profile with pre-welding with five spots.

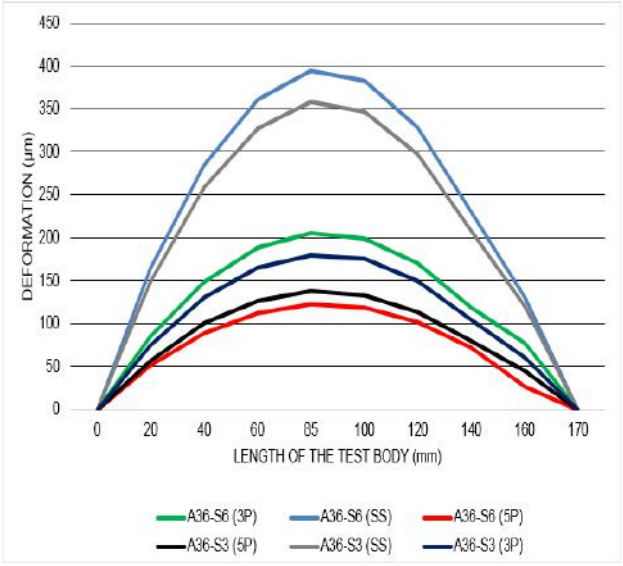

Fig. 5 - Longitudinal deformation at the cross-section indicated by the red arrow in Fig. 4. Legend: U profiles without preparation welded with AWS ER70S-3 (SS) or ER70S-6 (SS), U profiles with three spot-welds preparation welded with AWS ER70S-3 (3P) or ER70S-6 (3P), and U profiles with five spot-welds preparation welded with AWS ER70S-3 (5P) or ER70S-6 (5P).

Source: From the authors.

Fig. 6 illustrates the propagation of corrosion on the surface of the material, and its degradation. The welded part reaches the maximum degradation rate of 11 µm per year after 65 days, but it stabilises after that. Fig. 7 presents the result of the macrograph test that shows a reinforcement of the bead due to a good penetration of the weld. The weld bead widths were around 6.7 mm and 5.5 mm using AWS ER70S-3 and AWS ER70S-6 electrode wires, respectively.

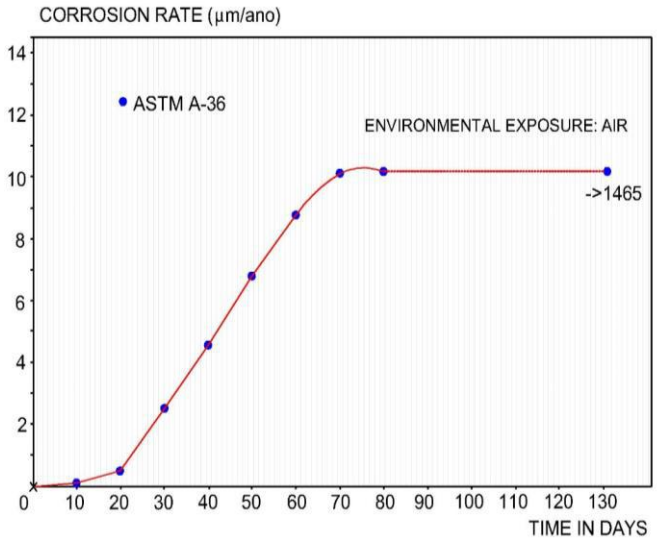

Fig. 6 - Corrosion rate diagram for ASTM A36 steels.

Source: From the authors.

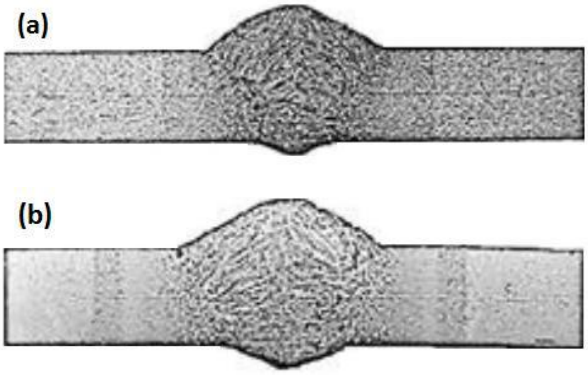

Source: From the authors.

Fig. 7 - Macrograph of welded joints for different sample sets of BM with weld metal; (a) sample welded with A36-S6 electrode and (b) sample welded A36-S3 electrode. Image scale: 50x.

Fig. 8 depicts microhardness measurements acquired in the cross-section of the welded joints, covering the Heat Affected Zone (HAZ) and the Base Metal (BM), Fine-Grained region (FG), Coarse-Grained region (CG), and the Welding Metal (WM). Maximum values will be found in the centre of the bead with an average of 185 Vickers, and it stabilises at 140 Vickers towards the base metal.

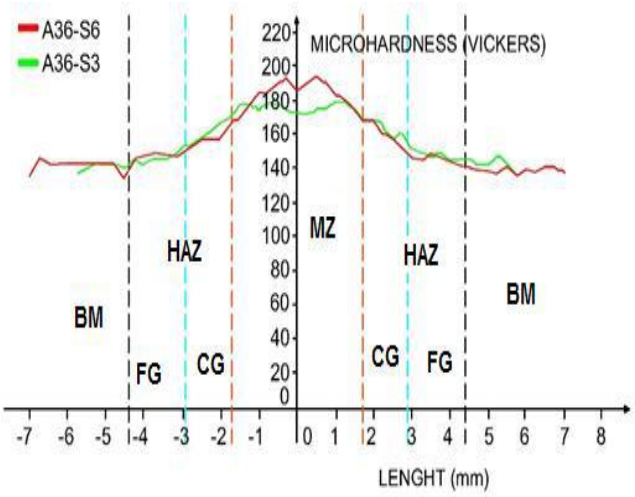

Fig. 8 - Microhardness curves for sets A36-S6 and A36-S3.

Source: From the authors.

Table 4 depicts the hardness values in the regions close to the weld bead and in the region of the thermally affected zone. In general, the values remained close to 150 Vickers, but increased by 17%, to 185 Vickers, in the weld bead.

Fig. 9 shows the result of the tensile tests. It can be noticed that all samples ruptured in the same region, on the border of the HAZ with the Base Metal. Table 5 depicts the average results from the tensile tests of the samples extracted from the weld bead region of A-36 steel of both ER70-S6 and ER70-S3 electrodes.

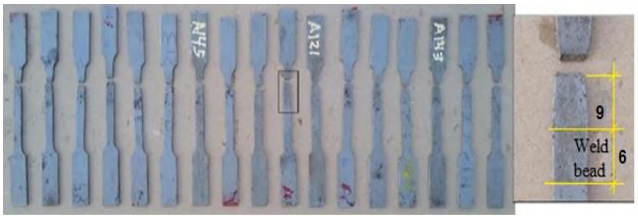

Fig. 9 - Breakage occurrence in HAZ: 9mm away from the bead.

Source: From the authors.

Table 4 - Mean Vickers values (HV) microhardness test measurements: base metal (BM); thermally affected zone (HAZ), fine-grained region (FG); coarse-grained region (CG); melting zone (MZ).

Sample	BM	HAZ	FG	CG	MZ	MZ/CG	CG/FG	MZ/HAZ	HAZ/BM
A36-S6	141	155	149	161	188	1.17	1.08	1.21	1.10
A36-S3	143	150	143	156	176	1.13	1.09	1.17	1.05

Source: From the authors.

Table 5 - Average values of displacement, strain, and breaking stress in a tensile test from the 90 samples extracted from the weld bead region of A-36 steel of both ER70-S6 and ER70-S3 electrodes.

Displacement	Strain	Breaking Stress
mm	**%**	**MPa**
15,77	9,3%	430,22

Source: From the authors.

IV. DISCUSSION

Structural steel profiles are widely used in industry and the construction of buildings. Most of the time, they are assembled using welded joints [1]. Although the welding process and its variables are widely known, industries still face several challenges when they have to assemble parts in situ, especially regarding misaligned and warped structural elements due to poor welding. There are some data on metallic structures collapsing due to poor welding quality [23][24]. There is, therefore, a need for a welding methodology, applicable in industry, that controls distortion and mechanical properties of the weld joints on structural profiles, ensuring the safety of the structure.

Consequently, this study aimed to analyse distortion, macro-structural corrosion, and microhardness of the most common steel profile used in metallic structures, the ASTM A36 cold-bent steel U profile, when it is welded with a new proposed welding methodology using a robotic arm assisted with real-time data acquisition of deformation levels. With this method, we hypothesize that it is possible to measure and control distortion, misalignment, and warping when assembling/welding those profiles in situ. In the current study, Gas-Shielded Arc Welding (GMAW) processes with two distinct electrode wire types and three joint preparation methods were employed.

Table 3 presented the basic chemical elements of the weld bead obtained by spectrometry technique. It shows that manganese and silica elements dissolved in the solder bead, which was similar to the welding procedure conducted by Venkateshkannan (2022) [13], but in flat steel sheets.

In terms of distortion/displacement due to thermal energy, Figures 4 and 5, the bent wings stabilised the structure, thus preventing larger profile distortions, either with AWS ER70S-6 or AWS ER70S-3 electrode wires. The average displacement in the wing was less than 200µm and less than 450µm at the centre of the profile. Figure 5 depicted the distortion of a cross-section of the profile: due to the distortion of crystalline planes in the bent wings, the heat did not propagate at the same speed as in the centre, thus resulting in less distortion. Such deformations agreed with the work of Baruah (2022), which presented larger displacements close to the weld regions due to thermal residual stresses.

Corrosion is another relevant parameter in welded joints of structural profiles. When internal forces derived from initial corrosion act on the cross-sectional area, they may exceed the ultimate failure stress, thus, gradually, and internally, increasing the erosion in the profile cross-sectional area. This is particularly important in ASTM A36 steel, as it is widely used in industry, and it is noticeably less corrosion-resistant than other steel alloys [25].

As shown in Figure 6, once the corrosion of ASTM A36 has started, the mass loss rises at a very slow pace, reaching 0,5 µm/year after 20 days. From this point, the corrosion rate abruptly increases and reaches a plateau of 10 µm/year around the 70th day. The main reason for the occurrence of a plateau is due to the surface oxide-saturation phenomenon in the cross-section area, which behaved as a shield and limited a further increase in the rate. Nonetheless, in comparison to the entire duration of the material degradation test (1465 days), the period of a sharp increase in the corrosion rate is very short, only 50 days. Silva, Costa, and Almeida investigated corrosion using cathodic protection in thick ASTM A36 steel plates, and they found similar rates of cross-sectional area loss during the salt spray acceleration process [16].

The macrograph in Figure 7 pictures a good reinforcement of the joint and a homogeneous cross-section throughout the length of the bead, either for a profile welded with A36-S6 or A36-S3. The only, and minor, difference was in the width of the HAZ. This gives confidence that the welding robot was efficient in welding those profiles.

In terms of hardness, Figure 8, regions with lower hardness and better preservation of the base metal were observed when electrode AWS ER70-S3 was used. This might be a result of an ideal heat input rate, as there was a larger weld bead (fusion zone), and the chemical elements were more diluted compared to the weld bead with AWS ER70-S6, Table 3. Moreover, the welding beads' macrography in Figure 7 shows the formation of long crystals in the specimen welded with ER76-S6 electrode wire, indicating a higher concentration of manganese in the ER76-S6 electrode wire, leading to an increase in hardness levels [18]. This indicates that electrode AWS ER70-S3 might be a better choice in welding ASTM A36 cold-bent steel U profiles, as it is necessary to have homogeneity in

the dilution of chemical elements and lower hardness, and electrode AWS ER70-S3 might be best suited for welding anchor bolts, as it is needed stiffer joints in this case.

In terms of mechanical properties and breaking behaviour acquired from the tensile tests, Figure 9 and Table 5, it was possible to notice that the rupture of every specimen followed the pattern shown in Figure 9, which might be related to the hardness and ductility changes in the material in this fractured region. As can be seen in Figures 7 and 8, the fracture occurred in the transition between the HAZ and base metal zones, where the hardness levels dropped to 140 Vickers, a much softer region.

V. CONCLUSION

The aim of this study was to propose a new welding methodology for the ASTM A36 steel U profiles using a robotic arm assisted with real-time data acquisition of deformation levels. With this method, it is possible to reduce distortion, misalignment and warping when assembling those profiles in situ. The use of laser scanning on the welded surfaces allowed to model and measure the distortions caused by the welding process, with an accuracy 160 microns between different readings. This distortion analysis process might be a useful tool for industries that use the GMAW welding process. Future studies will be to employ this technique into other structural profiles and other electrodes.

DECLARATION OF INTERESTS

The authors declare that they have no known competing financial interests or personal relationships that could have appeared to influence the work reported in this paper.

AUTHOR CONTRIBUTIONS

All authors contributed to the study conception and design. Material preparation, data collection and analysis were performed by Josemairon Prado Pereira, Bruno Agostinho Hernandez, Gilberto de Magalhães Bento Gonçalves and Edson Antonio Capello Sousa. The first draft of the manuscript was written by Josemairon Prado Pereira and all authors commented on previous versions of the manuscript. All authors read and approved the final manuscript.

ACKNOWLEDGMENTS AND FUNDING INFORMATION

The authors thanks the Graduate Program in Mechanical Engineering at UNESP – Campus of Bauru, Brazil. This project was funded by CadSteel Engenharia.

REPLICATION OF RESULTS

The results data will be made available as requested by anyone.

REFERENCES

[1] Majid G, Shervin M. (2023). Experimental and numerical investigations of block shear failure in gusset plates welded to double angle members. Structures., vol 48, 2023, p.1356-1372. Elsevier. https://doi.org/10.1016/j.istruc.2023.01.047.

[2] Akhyar; Tamlicha, A.; Farhan, A.; Azwinur; Syukran; Fadhilah, T.A.; Firsa, T.; Raja Ghazilla, R.A. Evaluation of Welding Distortion and Hardness in the A36 Steel Plate Joints Using Different Cooling Media. Sustainability 2022, 14, 1405. https://doi.org/10.3390/su14031405.

[3] M. V. Deo & P. Michaleris (2003) Mitigation of welding induced buckling distortion using transient thermal tensioning, Science and Technology of Welding and Joining, 8:1, 49-54, DOI: 10.1179/136217103225008919.

[4] Hasan MF (2016) Analysis of Mechanical Behavior and Microstructural Characteristics Change of ASTM A-36 Steel Applying Various Heat Treatment. J Material Sci Eng 5: 227. doi:10.4172/2169-0022.1000227

[5] Azad, N., Darvazi, A.R. & Iranmanesh, M. Effect of Thermal Distribution and Stiffness Variation on Welding Distortion in a Ship Panel Structure. Arab J Sci Eng 44, 10373–10387 (2019). https://doi.org/10.1007/s13369-019-04043-x

[6] Nandakumar, N., and K. S. Yokesh. "Experimental validation and Parametric Optimization in MIG welding of A-36 steel plate using Taguchi-Fuzzy logic approach." Solid State Technology 64.2 (2021): 5547-5561.

[7] Pushp Kumar Baghel, Effect of SMAW process parameters on similar and dissimilar metal welds: An overview, Heliyon, Volume 8, Issue 12, 2022, e12161, ISSN 2405-8440, https://doi.org/10.1016/j.heliyon.2022.e12161.

[8] Brownell, Lloyd E., and Edwin H. Young. Process equipment design: vessel design. John Wiley & Sons, 1959, ISBN: 978-0-471-11319-5.

[9] Millet, Barry, et al. "ASME Pressure Vessel Internals and Their Design Code." Pressure Vessels and Piping Conference. Vol. 56963. American Society of Mechanical Engineers, 2015. https://doi.org/10.1115/PVP2015-45312.

[10] Fatima, Shane & Khan, Mushtaq & Jaffery, Syed & Ali, Liaqat & Mujahid, Mohammad & Butt, Shahid. (2015). Optimization of process parameters for plasma arc welding of austenitic stainless steel (304 L) with low carbon steel (A-36). Proceedings of the Institution of Mechanical Engineers, Part L: Journal of Materials: Design and Applications. 230. 10.1177/1464420715584392.

[11] Sagar Ashvinkumar Padhiar, S. Vincent, Effect of hard facing processes on Mild steel A-36 by arc welding,

Materials Today: Proceedings, Volume 28, Part 2, 2020, Pages 526-531, ISSN 2214-7853, https://doi.org/10.1016/j.matpr.2019.12.213.

[12] R.A. Bajares, L. Di Mella, Study of the Corrosion Rate in the Couple of Steels ASTM A-36 and AISI/SAE 304 in a Water-coke of Petroleum System., Procedia Materials Science, Volume 8, 2015, Pages 702-711, ISSN 2211-8128, https://doi.org/10.1016/j.mspro.2015.04.127.

[13] Venkateshkannan M, Arivazhagan N, Nageswara Rao M, Madhusudhan Reddy G. Characterization of weld joints produced by continuous wave and double pulse gas metal arc welding in naval grade high-strength low-alloy steel [online]. Proceedings of the Institution of Mechanical Engineers Part E: Journal of Process Mechanical Engineering 2022. doi: 10.1177/09544089221126430.

[14] Akhyar, Akhyar & Akram, Akram & Farhan, Ahmad & Azwinur, & Syukran, & Fadhilah, Teuku & Firsa, Teuku & Raja Ghazilla, Raja Ariffin. (2022). Evaluation of Welding Distortion and Hardness in the A36 Steel Plate Joints Using Different Cooling Media. Sustainability. 14. 1405. 10.3390/su14031405.

[15] Baruah, Sandipan & Sarkar, Subrato & Singh, Indra Vir & Mishra, B.K. (2022). A computational framework based on FEA, ML and GA for estimation of welding residual stresses. Finite Elements in Analysis and Design. 205. 10.1016/j.finel.2022.103753.

[16] Silva, Adiana & Costa, Esdras & Almeida, José & Maciel, Theophilo & Cavalcante, Danielle & Passos, Tibério. (2022). Effect of Hydrogen on the Mechanical Properties of ASTM A182 F22 and ASTM A36 Steels Welded Joint Using Inconel 625 as Filler and Buttering Metal. Materials Research. 25. 10.1590/1980-5373-mr-2021-0339.

[17] Ma, Hong & Qin, Guoliang & Geng, Peihao & Ao, Zhiyong & Chen, Yong. (2022). Effect of intermetallic compounds on the mechanical property and corrosion behaviour of aluminium alloy/steel hybrid fusion-brazed welded structure. Journal of Manufacturing Processes. 75. 170-180. 10.1016/j.jmapro.2022.01.004.

[18] Coelho, Fagner & Bracarense, Alexandre & Lima II, Eduardo. (2022). Analysis of Parameters Based on Deposited Beads Geometry in Single-Pass Multi-layers Applied in Wire Arc Additive Manufacturing Process. Arabian Journal for Science and Engineering. 10.1007/s13369-022-07011-0.

[19] John M, P AK, K UB. AHSS welding using undermatching filler wires and process advantages with P-GMAW. Materials Today: Proceedings. Proceedings, and undefined. 2022;49:1312-8. doi: 10.1016/j.matpr.2021.06.388.

[20] Subashini, L. & Prabhakar, K. & Ghosh, Swati & Gadhe, Padmanmabham. (2020). Comparison of laser-MIG hybrid and autogenous laser welding of M250 maraging steel thick sections—understanding the role of filler wire addition. The International Journal of Advanced Manufacturing Technology. 107. 10.1007/s00170-020-05113-3.

[21] AMERICAN SOCIETY FOR TESTING AND MATERIALS. ASTM-B117-11: Standard practice for operating salt spray (fog) apparatus, West Conshohocken, 2011.

[22] BRITISH STANDARD – GROUP BSI. BS 709:1983: Procedures for UK registration for open systems standards. Procedures for the UK name registration authority, United Kingdom, 1991.

[23] Masabuchi, Koichi, Analysis of Welded Structures (Pergamon International Library: International series on materials science and technology; 33), USA, 1980.

[24] RONG, Y.; HUANG, Y.; WANG, L. Evolution Mechanism of Transient Strain and Residual Stress Distribution in Al 6061 Laser Welding. Crystals, Basel, v. 11, n. 2, p. 13, 17 February 2021. ISSN 2073-4352. Disponivel em: <https://www.mdpi.com/2073-4352/11/2/205>. Acesso em: 13 March 2021. Considering the harm that residual stress causes to the mechanical properties of a weld joint, the evolution mechanisms of transient strain and residual stress distribution are investigated in laser welding of Al 6061, considering that these originate fro.

[25] SEIDU, S. O.; KUTELU, B. J. Effect OF HEAT TREATMENTS ON CORROSION OF WELDED LOW-CARBON STEEL IN ACID AND SALT ENVIRONMENTS. Journal of minerals and materials characterization and engineering, Ado-Ekiti, v. 1, n. 2013, p. 95-100, may 2013.